PI-based controller for low-power distributed inverters to maximize reactive current injection while avoiding over voltage during voltage sags

Jaume Miret [1*], Miguel A. Garnica[1], Miguel Castilla[1], Jose Luis Garcia de Vicuña[1], Antonio Camacho[2]

[1] Departament d'Enginyeria Electrònica, Universitat Politècnica de Catalunya (UPC), Avda. Victor Balaguer s/n , Vilanova i la Geltrú, 08800 Barcelona, Spain.
[2] Department of Automatic Control, UPC, Avda. Victor Balaguer s/n, Vilanova i la Geltrú, 08800 Barcelona, Spain.
[*] jmiret@eel.upc.edu

Abstract: In the recently deregulated power system scenario, the growing number of distributed generation sources should be considered as an opportunity to improve stability and power quality along the grid. To make progress in this direction, this work proposes a reactive current injection control scheme for distributed inverters under voltage sags. During the sag, the inverter injects, at least, the minimum amount of reactive current required by the grid code. The flexible reactive power injection ensures that one phase current is maintained at its maximum rated value, providing maximum support to the most faulted phase voltage. In addition, active power curtailment occurs only to satisfy the grid code reactive current requirements. As well, a voltage control loop is implemented to avoid overvoltage in non-faulty phases, which otherwise would probably occur due to the injection of reactive current into an inductive grid. The controller is proposed for low-power rating distributed inverters where conventional voltage support provided by large power plants is not available. The implementation of the controller provides a low computational burden because conventional PI-based control loops may apply. Selected experimental results are reported in order to validate the effectiveness of the proposed control scheme.

1. Introduction

Traditionally, grid power-quality has been supported by large synchronous generators in conventional power plants and by hardware compensators located in certain nodes. Nowadays, the growing number of spread renewable energy sources should be considered as an opportunity to improve stability and power quality along the grid [1]–[8]. In addition, in some countries, transmission systems present a high and rising dependence on grid-connected distributed generation sources (DGS). In order to guarantee the stability and reliability of the power system, DGS continuous-operation during network disturbances is required in international standards and national grid codes [2]–[5]. During severe disturbances, DGS must follow stringent rules related to low-voltage ride-through (LVRT) and reactive current injection (RCI) protocols [6]–[8]. LVRT protocols establish voltage boundaries for the continuous operation of the DGS in the point of common coupling (PCC). When any of the phase voltages goes outside the limits, DGS must be disconnected after a predefined trip-time. On the other hand, national grid codes require some reactive power injection during voltage sags in order to support the grid according to different protocols [6].

One of the most common and challenging disturbances are voltage sags, defined as an undesired and transitory amplitude reduction in one or more phases [9]–[10]. Due to the rigorous continuous-operation requirements of DGS during voltage sags, several problems may appear. To start with, the reactive power capacity of full-power inverters is limited by a maximum rated current that must not be surpassed. Hence, the first problem arises when trying to maintain the pre-sag active power injection or to inject the reactive power required by grid codes, since inverters may suffer undesired overcurrents in one or more phases. To overcome this problem, combined positive and negative-sequence RCI protocols have been proposed in different studies [11]–[16]. Contributions [14] to [20] also provide additional functionalities during unbalanced voltage sags, for example, a reduction of the dc-link oscillations.

The second well-known issue in RCI protocols is the voltage support capability they offer in mainly inductive grids [17], [21]–[30]. The proposal of [17] is based on controlling the amplitude and phase angle of the negative-sequence current to minimize the negative-sequence voltage. The approach in [21] presents a combined positive and negative-sequence RCI protocol that provides flexible voltage support without requiring closed-loop control. A similar scheme is used in [22] to explore the effect of active power injection in resistive grids. Several works [23]–[28] propose different controllers based on the injection of positive and negative-sequence with the aim of restoring the faulted phase voltages back into the limits of continuous operation. References [23] and [24] propose controllers for high-power DGS with the aim of restoring the faulted phase voltages back into the limits of continuous operation.

In the context of low-power DGS, the voltage restoration proposed by the previous works may be of little use. In particular, the problem arises when dealing with sags that present high drop in one or two voltage phases while the others remain almost un-faulted [18], [19], [29] and [30]. In these cases, conventional RCI without additional voltage control may lead to overvoltage scenarios, causing tripping and blackouts. As a consequence, with low-power distributed inverters, control objectives must be different. They must be less ambitious than the reviewed RCI protocols and they must focus on maximizing the current injection of the inverters up to their maximum capabilities while avoiding surpassing the maximum voltage boundaries. Regarding the inverters, the fulfillment of these objectives provides optimal current injection profiles. With regard to the grid, required support during voltage sags is provided. It is important to note that some works have addressed these two problems separately (overcurrent and overvoltage), but only a few of them try to solve them simultaneously [29], [30].

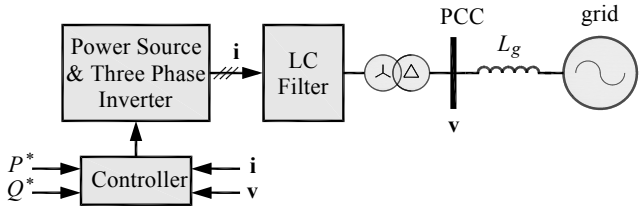

Fig. 1. Diagram of a grid-connected DGS.

The control scheme for low-power DGS in [29] ensures maximum reactive current injection in the most drooped phase, thus guaranteeing maximum support in this phase, while avoiding surpassing the maximum voltage limit. The main drawbacks of [29] are: 1) the control operates in open loop, and 2) an accurate estimation of the grid impedance is required for the correct operation of the proposal. In fact, inaccurate estimations of the grid impedance are going to introduce errors in voltages and currents, producing overvoltages and overcurrents in some cases. In addition, the calculation of the current references requires a complete active power curtailment, which is not mandatory in most of the grid codes [5], [7]. In addition, it requires a complex mathematical calculation of trigonometric functions and divisions that may lead to a high computational burden. A natural frame proportional voltage control based on German grid code requirements [8] was presented in [30]. In [30] the amount of RCI is calculated separately for each phase voltage, being proportional to each amplitude decrement. In this work, both active and reactive powers are injected simultaneously during the sag, giving preference to RCI through the implementation of an active current curtailment protocol. When one of the natural frame reference currents surpasses the maximum rated current, all the injected currents are reduced by the same proportional factor, thus ensuring overcurrent protection. In this proposal the injection of the maximum allowable reactive current is not an objective. In addition, the method used to avoid overvoltages is to make zero the reactive current in non-faulty phases, which presents the drawback of making also zero the voltage support to slightly dropped phases.

This work proposes a RCI scheme that overcomes the limitations of previous works while observing the RCI protocols defined in the Spanish grid code [4]. A relevant feature of the controller presented in this paper is that it reaches always the maximum rated current in the most faulted phase, thus providing maximum support to the grid. In addition, a voltage control loop is implemented to avoid overvoltage due to the reactive current injection in the non-faulty phase. Concerning active power curtailment, it is only performed when required by the grid code according to the sag profile. The implementation of the control system requires a low computational burden because it is based on conventional PI control loops. The main contribution of this work is a control scheme that joins hierarchically four objectives: 1) fulfill LVRT reactive current injection requirements; 2) maintain pre-sag active power injection if first objective fulfillment permits it, and/or overcurrent is not reached; 3) use a PI controller to inject maximum rated reactive current in the most faulty phase; and 4) use a second PI controller to avoid overvoltage due to the reactive current injection. As far as authors know, there is not any closed loop controller applied to the complex problem of fulfilling these four objectives at the same time. Reaching these control objectives coordinately implies addressing additional problems, and thus requires developing new control algorithms. Additionally, when fulfilling these objectives simultaneously, some interactions appear and it has not been reported in the literature.

The paper is organized as follows. Section 2 describes the DGS behavior during voltage sags. Section 3 presents the control objectives and the proposed control algorithm. Section 4 develops some design guidelines to obtain the controller parameters. Section 5 corroborates experimentally the expected features. Section 6 presents a comprehensive comparison with previous state-of-the-art solutions. Section 7 concludes the work.

2. Grid-connected inverters under voltage sags

This section describes grid-connected DGS.

2.1.Grid-connected Three-phase Inverter

The diagram of a DGS connected to the PCC through a fully rated three-phase three-wire inverter is shown in Fig. 1. The inverter output stage consists on an LC filter connected to the PCC through a wye-delta transformer. The parasitic inductance of this transformer works as output inductance of an equivalent LCL filter. Inductor L_g models a mainly inductive line between the PCC and the grid. The main objective of the inverter is to inject the active power P_G generated by the DGS into the grid. The reference active power value P^* is provided by an external controller with the aim of maximizing power generation in the source (i.e. maximize P_G), which can be wind or photovoltaic prime movers. As an ancillary service, reactive power Q^* can be also required by the grid operator to support the grid voltage.

2.2.Voltage Sag Characterization

Due to the hardware configuration used in Fig. 1 the instantaneous PCC phase voltages **v** can be described as the addition of positive and negative symmetric sequences in the stationary reference frame (SRF) as

$$v_\alpha = v_\alpha^+ + v_\alpha^- = V^+ \cos(\omega t) + V^- \cos(\omega t + \delta) \quad (1)$$

$$v_\beta = v_\beta^+ + v_\beta^- = V^+ \sin(\omega t) - V^- \sin(\omega t + \delta) \quad (2)$$

where v_α^+, v_β^+ and v_α^-, v_β^- are the SRF positive and negative voltage sequences respectively, V^+ and V^- are their amplitudes, ω is the grid angular frequency, and δ is the phase angle between positive and negative-sequence [21].

2.3. Current Injection During Voltage Sags

According to the instantaneous power theory, the active power p and reactive power q injected into the grid by a three-phase inverter can be defined as:

$$p = \frac{3}{2}(v_\alpha i_\alpha + v_\beta i_\beta) \quad (3)$$

$$q = \frac{3}{2}(-v_\beta i_\alpha + v_\alpha i_\beta)\,. \quad (4)$$

The reference currents can be derived by ensuring that the instantaneous powers track their references P^* and Q^*, assuming that the inner current control loop is properly tuned

(i.e. there is a perfect matching between the reference and the generated current, $\mathbf{I} = \mathbf{i}^*$). Then, the reference currents can be decomposed into active and reactive components

$$i_\alpha^* = i_\alpha^*(p) + i_\alpha^*(q) \tag{5}$$

$$i_\beta^* = i_\beta^*(p) + i_\beta^*(q)\,. \tag{6}$$

The reference currents can be defined as [13], [24]

$$i_\alpha^* = \frac{I_p}{V^+} v_\alpha^+ + \frac{I_q^+}{V^+} v_\beta^+ + \frac{I_q^-}{V^-} v_\beta^- \tag{7}$$

$$i_\beta^* = \frac{I_p}{V^+} v_\beta^+ - \frac{I_q^+}{V^+} v_\alpha^+ - \frac{I_q^-}{V^-} v_\alpha^- \tag{8}$$

where I_p is the active power component of the reference currents, and I_q^+, I_q^- are the reactive positive and negative-sequence components. The value of I_p is related to the generated active power P_G. By adequately balancing the two reactive current components I_q^+ and I_q^-, reactive power injection will have different effects on the grid, as shown in Section III.

3. Formulation of control objectives and proposed control algorithm

The aim of this section is to define the control objectives and to develop the control algorithm that allows the efficient implementation of these objectives.

3.1. Control Objectives

The proposed control objectives of the DGS during voltage sags are listed below.

- Objective 1: To fulfill the RCI requirements of Spanish grid code (see Fig. 2):

$$\frac{I_q}{I_{rated}} \geq \frac{I_{q\_min}}{I_{rated}}\,, \tag{9}$$

where I_q is the reactive current amplitude, I_{rated} is the inverter maximum allowable current, and $I_{q\ min}$ is the minimum current required by the grid code during the sag.

- Objective 2: To maintain the active power injection to pre-sag values:

$$P^* = P_G\,. \tag{10}$$

This objective is usually not defined by grid codes and thus different approaches can be found in current literature when dealing with active power during a voltage sag. Some works set a complete active power curtailment during the sag in order to improve RCI ([18], [24], [25], and [29], among others). Other approaches provide only active power curtailment when it is mandatory to observe the minimum ratio of RCI ([13], [14], [16], [22], and [30]). In this work, objective 2 has been chosen to ensure a fast return to normal conditions. When the system recovers from the sag a quick return to pre-sag active power generation is a requirement to ensure fair power balance and frequency stability [31].

- Objective 3: To inject the maximum current in order to further improve the voltage support capabilities:

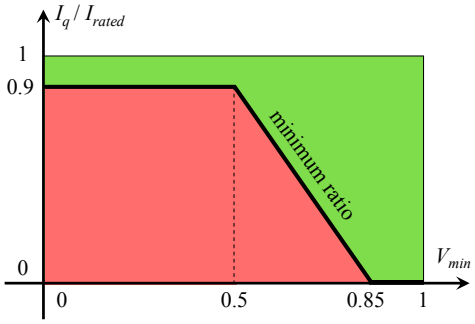

Fig. 2. Proposed reactive current injection requirement (in p.u.) adapted from Spanish grid code [4].

$$\max\{I_a, I_b, I_c\} = I_{rated}\,. \tag{11}$$

being I_a, I_b and I_c the amplitudes of the phase currents.

- Objective 4: To avoid overvoltage in the phase voltage with higher amplitude:

$$\max\{V_a, V_b, V_c\} \leq 1.1 \text{ p.u.} \tag{12}$$

3.2. Proposed Control Strategy

To accomplish the control objectives, the proposal of this work is to adapt the Spanish grid code in terms of reactive current injection [4] to obey the logics shown in Fig. 2. In this code, the ratio between reactive and total current I_q /I_T must be always inside the green zone. Two changes can be noted in the figure. First, I_q/I_T in the code has been changed into I_q /I_{rated}. Then, the inverter must inject "all" its available current during the sag. And secondly, the generic "voltage at PCC" in the code has been changed into V_{min}, i.e. the minimum voltage in case of unbalanced faults. The minimum voltage has been chosen because in case of unbalanced faults, it identifies the most dropped phase, thus indicating the phase that requires more support.

The accomplishment of the proposed objectives presents some drawbacks that will be described below using simulation examples. Fig. 3 shows four examples of reactive current injection strategies during the same sag in different low active-power production scenarios: connected to a weak grid [32], [33] (L_g = 0.07 p.u. in a system with base power 1.4 kVA) or to a stiff grid (L_g = 0.007 p.u.), and with different reactive current injection protocols (see Table 1). Top figures show the PCC phase voltages amplitudes in p.u. Two dashed lines at 1.1 p.u. and 0.85 p.u. are drawn to highlight the voltage boundaries for normal operation [2]. Bottom figures show the phase current amplitudes for each scenario. The maximum rated current has been chosen as I_{rated} = 1 p.u., which is shown as a horizontal dashed line in the figure. Fig. 3 (a) shows the phase voltage amplitudes and injected phase currents during a voltage sag in a stiff grid (low grid-inductance value). Before t = 0.1 s, the phase voltages are at their nominal amplitude 1 p.u. Bottom figure shows the current amplitudes of the inverter, which are balanced at 0.48 p.u before the sag. Thus, in this case, the active power production is roughly 50% of the peak production. At t = 0.1s, a sag occurs and two phase voltages drop below the minimum operation boundary. Then, the amplitude of the injected active currents increases to 0.56 p.u., in order to

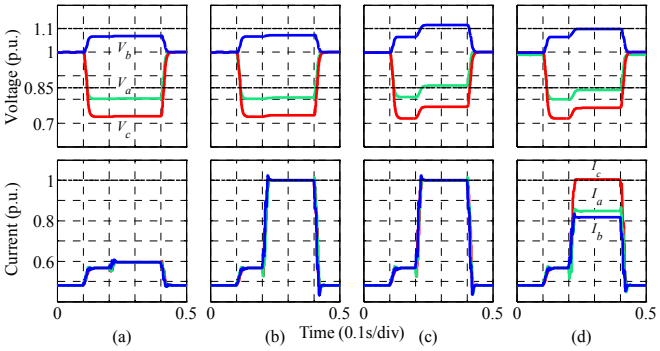

Fig. 3. Different reactive injection strategies in a low active-power production scenario. Top: PCC phase voltage amplitudes, bottom: current amplitudes. The simulation scenarios (a), (b), (c) and (d) are detailed in Table 1.

Table 1. Conditions for scenarios of Fig. 3.

	grid stiffness	maximum current	overvoltage control	reactive control protocol
a	stiff	No	No	$I_q^+>0, I_q^-=0$
b	stiff	Yes	No	$I_q^+>0, I_q^-=0$
c	weak	Yes	No	$I_q^+>0, I_q^-=0$
d	weak	Yes	Yes	$I_q^+>0, I_q^->0$ **proposed**

maintain the pre-sag active power injection. It must be noted that the reactive injection protocol remains intentionally inactive from $t = 0.1$ s to $t = 0.2$ s in order to clearly show the sag profile. At $t = 0.2$ s, a positive-sequence reactive current injection strategy to accomplish the minimum ratio I_q/I_T begins [4], with I_T reaching a peak value of 0.6 p.u., far below the maximum allowable current $I_{rated} = 1$ p.u. A small balanced increment in all the PCC voltages can be noticed. This increment is due to the low value of the grid inductance.

Fig. 3 (b) shows the same scenario (low grid inductance value and low active-power production) but with a strategy that maximizes the reactive current injection. As it can be seen, at $t = 0.21$ s, I_{rated} is reached, maintaining the pre-sag active power injection and delivering all the remaining current as positive-sequence reactive current ($I_q = 0.82$ p.u.). A slightly higher voltage increment can be noted in the PCC voltages, thus showing a better support to the sag conditions. This would be the ideal scenario where the proposed objectives are accomplished simultaneously.

Fig. 3 (c) considers a weak grid scenario in which the grid inductance is higher than in the previous two tests. In this case, the higher positive-sequence reactive current produces the undesired effect of an overvoltage on the unfaulted phase *b* which exceeds the top boundary for continuous operation. This situation could be avoided reducing the reactive current injection. In that case, the injected total current would be below I_{rated}, thus, the maximization of the capabilities of the inverter would not be achieved. Then, the reactive current injection strategy must be improved to avoid this circumstance.

Fig. 3 (d) shows the same scenario than in (c) but with the improved reactive current injection strategy that maximizes the capabilities of the inverter avoiding overvoltages. Maximizing the voltage support capability of the inverter is done through injecting maximum rated current in the phase with deeper voltage drop. Avoiding overvoltages in the non-faulty phase/s is done ensuring minimum reactive

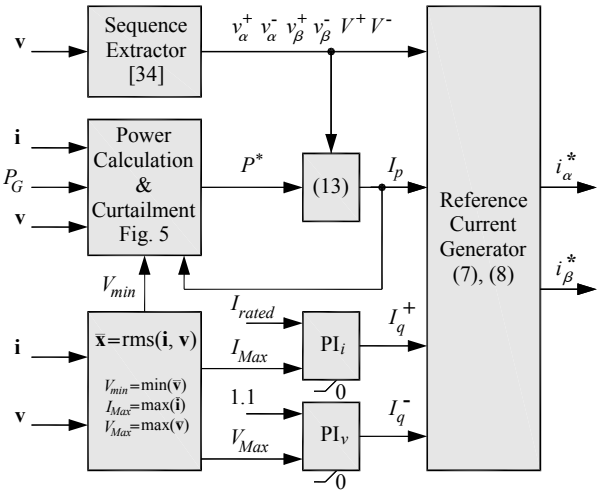

Fig. 4. Block diagram of the proposed control scheme.

current injection in the phase/s with lower voltage drop. In this sense, when an unbalanced sag occurs, the most perturbed phase receives maximum reactive current and the less perturbed phase receives its minimum reactive current. These issues can be clearly seen in the simulation: to avoid overvoltage in phase *b*, the reactive current injection is made from both positive and negative-sequence, which produces a raising and equalizing effect over the PCC voltages. Also, due to the combined effect of positive and negative-sequence reactive currents, the phase currents are clearly unbalanced. The maximum current (equal to I_{rated}) is reached in the most dropped phase *c* (red), i.e. providing maximum support in this phase voltage. The minimum phase current *b* produces the minimum voltage increment (as desired), which places the phase *b* voltage just at the upper-voltage limit. Analyzing Fig. 3 (d) it can be clearly noted that the objective of maximizing the voltage support capabilities of the inverter while avoiding the drawback of over-passing the continuous operation limits can be fulfilled.

3.3. Proposed Control Scheme

To obtain the proper components (I_p, I_q^+ and I_q^-) for the reference currents generator (7) and (8), the functionality of each component must be analyzed. On one hand, I_p is responsible for injecting the active power to the grid (objective 2). On the other hand, I_q^+ equally contributes to raising all the phase currents [21]. Consequently, I_a^+ is chosen to bring the maximum phase current I_{Max} to the rated current value I_{rated} (objective 3). The last component, I_a^-, equalizes current amplitudes [21], i.e. it reduces the maximum current and increases the minimum current. As a result, it reduces the maximum voltage increment over the grid inductance and it can be used to avoid overvoltage at the phase with maximum amplitude V_{Max} (objective 4).

Fig. 4 shows the block diagram of the controller that fulfills the proposed functionalities. First, a sequence extractor based on cascaded second order generalized integrators (SOGI) [34] is used in order to obtain the voltage sequences of the PCC voltages, which will be used in the reference current generator (7) and (8).

The reference active power P^* is provided by the power calculation & curtailment block. This block, which is responsible for achieving objectives 1 and 2, will be

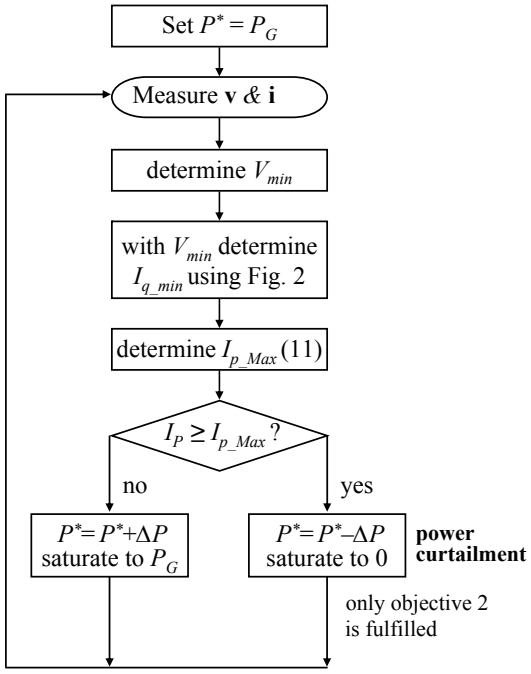

Fig. 5. Proposed flowchart for the power curtailment function.

described in detail below. I_p is obtained by dividing P^* by the voltage positive-sequence amplitude V^+

$$I_P = \frac{2}{3}\frac{P^*}{V^+}. \tag{13}$$

Note that a different approach for the management of active power is also compatible with the control algorithm proposed here. For instance, a complete active power curtailment during the sag is possible by setting $I_p = 0$. Even in this case, the control algorithm will still operate correctly. A PI controller is used to determine the reactive-current positive-sequence component I_q^+ and it is responsible for carrying out objective 3. This PI forces the current with maximum amplitude I_{Max} of the measured current vector **i** to be equal to the maximum allowed current I_{rated}. I_{Max} is calculated using an algorithm that computes the root mean square (rms) values of the current vector **i** and determines its maximum. Forcing the maximum current to be equal to I_{rated} provides maximum voltage support during the voltage sag. This PI is saturated to a minimum value of zero, avoiding leading reactive current during the sag.

A second PI controller is used to determine I_q^-, which is responsible for balancing the PCC voltages. This balancing will produce a reduction in the higher phase voltage and a raise in the lower phase voltage, thus avoiding overvoltage due to I_q^+. The inputs of this controller are the maximum amplitude of the phase voltages V_{Max} and the upper-voltage boundary for continuous operation, 1.1 p.u. V_{Max} is obtained by both a rms algorithm over the voltage vector **v** and a simple comparison to determine the phase voltage with maximum amplitude. This PI is provided with a lower saturation level equal to zero, i.e. it begins working when the upper-voltage boundary is exceeded. When overvoltage does not occur, the PI output is set to $I_q^- = 0$, i.e. no negative-sequence is injected. The values of the controller parameters have been derived using small-signal modelling and stability analysis tools.

3.4. Active power curtailment

Table 2 System parameters

Parameter name	*Acr.*	Value
Grid voltage (line to neutral)	V_g	110 V rms
Grid frequency	f	60 Hz
DC-link voltage	V_{dc}	350 V
Nominal rated power (base power)	S_b	1.4 kVA
Rated current amplitude	I_{rated}	6 A
Generated active power	P_G	100 W and 1100 W
LC filter input inductances	L_i	5 mH, 0.073 p.u.
LC filter capacitances	C	1.5 μF, 0.015 p.u.
LC filter damping resistors	R_d	68 Ω, 2.623 p.u.
Transformer equivalent inductance	L_o	2 mH, 0.029 p.u.
Grid inductance	L_g	5 mH, 0.073 p.u.
Increment for power curtailment	ΔP	0.01 p.u.
RMS filter window-width	T_w	16 ms
Proportional gain V_{Max} compensator	k_{p_v}	0.45 A V^{-1}
Integral gain V_{Max} compensator	k_{i_v}	16 A $(V\ s)^{-1}$
Proportional gain I_{Max} compensator	k_{p_i}	0.6
Integral gain I_{Max} compensator	k_{i_i}	130 s^{-1}
Proportional gain PRES current compensator	k_p	10 A^{-1}
Integral gain PRES current compensator	k_i	30 $(A\ s)^{-1}$
Sampling and switching frequency	f_s	10 kHz

This subsection proposes a control algorithm for calculating the reference power P^*, including a power curtailment function. The proposal is based on a simple searching function, thus avoiding complex and time-consuming approaches.

The flowchart for this function is depicted in Fig. 5. During nominal operation, P^* is set to the power that is being generated by the renewable source, P_G (objective 2). When the sag is detected, the algorithm starts. First, the minimum amplitude of the phase voltages V_{min} is identified and it is used with Fig. 2 to calculate the minimum reactive current $I_{q\ min}$. This current guarantees the accomplishment of the grid code requirements (objective 1). When only positive-sequence of active and reactive currents are injected, the total injected current is

$$I_T = \sqrt{I_p^2 + \left(I_q^+\right)^2}. \tag{14}$$

The requirement for maximizing the capabilities of the inverter implies that the current must reach the maximum allowable current $I_T = I_{rated}$ (objective 3). To this end, the maximum value of the active current component is easily calculated with I_{q_min}

$$I_{p\_Max} = \sqrt{I_{rated}^2 - I_{q\_min}^2}. \tag{15}$$

This value is the maximum active current component that ensures that 1) the minimum ratio required by grid code is observed, and 2) no overcurrent is produced due to the active power generation during the voltage sag. As a consequence, power curtailment will take place if the active current component I_p is higher than the value I_{p_Max}. In this work, power curtailment is carried out by reducing the reference active power. Such reduction is performed by a predetermined power increment ΔP each time the flowchart is executed.

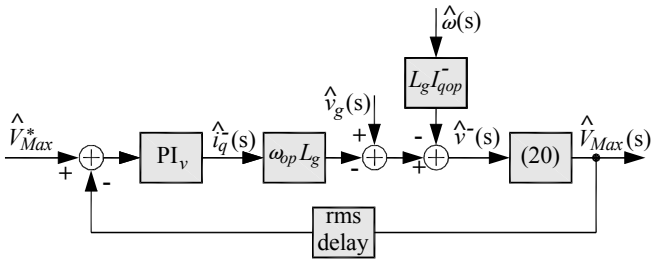

Fig. 6. Negative-sequence reactive-current control diagram.

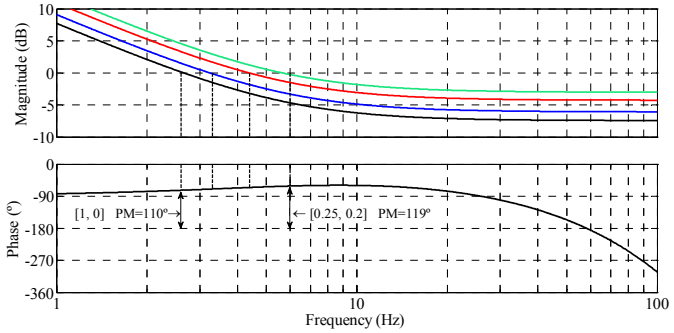

Fig. 7. Bode plot of the maximum-voltage loop gain for four different sags: [V_{op}^+, V_{op}^-] = {[1, 0] [0.8, 0.1] [0.5, 0.2] [0.25, 0.2]} p.u.

4. Design guidelines for the control loops

In this section, small-signal models for the maximum voltage loop and maximum current loop are developed in order to find the PI parameter values that guarantee system stability.

4.1. Maximum voltage loop

The large-signal expression of the PCC negative-sequence voltage when injecting negative-sequence reactive current can be written as [24]

$$V^- = V_g^- - \omega L_g I_q^- \tag{16}$$

being V_g the grid voltage amplitude. From (16), the small-signal model is derived as

$$\hat{v}^-(s) = \hat{v}_g^-(s) - \omega_{op} L_g \hat{i}_q^-(s) - L_g I_{qop}^- \hat{\omega}(s) \tag{17}$$

where "^" denotes small-signal components and subscript $_{op}$ denotes operating point values. Fig. 6 shows that the maximum voltage loop relates to I_q^- and to the rms value of the natural frame voltage with maximum amplitude. From (1) and (2), the amplitudes of the natural frame voltages can be written as a function of V^+, V^-, and the sequence phase angle of each phase $\phi = \{\delta, \delta - 2/3\pi, \delta + 2/3\pi\}$ as

$$V_{a,b,c} = \sqrt{\left(V^+\right)^2 + \left(V^-\right)^2 + 2V^+V^-\cos(\phi)}\,. \tag{18}$$

Hence, from (1) it follows that the phase voltage with maximum amplitude V_{Max} is the phase that presents the maximum cosine value cos_M

$$cos_M = \max\left\{\cos(\delta), \cos(\delta - {}^2/_3\,\pi), \cos(\delta + {}^2/_3\,\pi)\right\}. \tag{19}$$

Linearizing (18) around the operating point, a small-signal approximation to this non-linear function is obtained

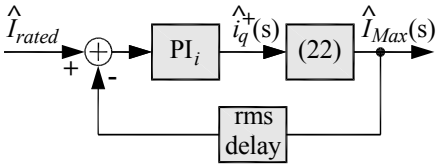

Fig. 8. Positive-sequence reactive-current control diagram.

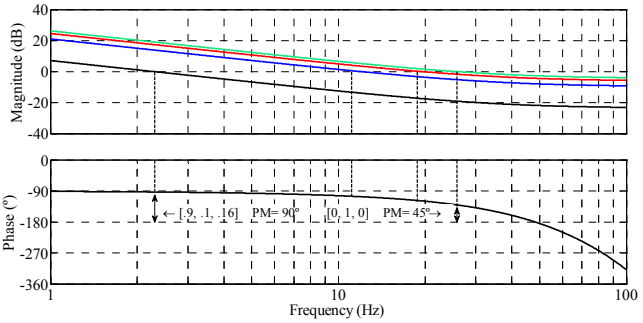

Fig. 9. Bode plot of the positive-sequence reactive-current loop gain for different current component values [$I_{p\,op}$, $I_q^+{}_{op}$, $I_q^-{}_{op}$] = {[0.9, 0.1, 0.16] [0.6, 0.4, 0.42] [0.4, 0.6, 0.42] [0, 1, 0]} p.u.

$$\hat{V}_{Max}(s) = \frac{V_{op}^- + V_{op}^+ cos_{M\,op}}{\sqrt{\left(V_{op}^+\right)^2 + \left(V_{op}^-\right)^2 + 2V_{op}^+V_{op}^- cos_{M\,op}}}\,\hat{v}^-(s) \tag{20}$$

Fig. 6 shows the block diagram of the small-signal model for this control loop. To measure the rms value of the voltage amplitude, an integral-based sliding window filter, with a window-width of a grid-period, is used. Taking into account that the output of Fig. 6 is already amplitude, only the delay of the rms filter must be modeled. Its small-signal model is implemented using an 8th *Pade* approximation [35].

Using the loop gain Bode plot, PI controller parameters are obtained by considering the worst-case scenario, which implies considering different operating points for (20). It must be noted that the positive/negative-sequence phase angle value has almost no influence in this analysis because its maximum value cos_M is always used. By choosing a low cross-over frequency and a phase margin PM = 110º for the worst case scenario (i.e. V_{op}^+=1, V_{op}^-=0), the following PI gains are derived: $k_{p\,v}$ = 0.45 A V^{-1} and $k_{i\,v}$ = 16 A $(V\,s)^{-1}$. Fig. 7 shows the Bode plots of the loop gain for different sags. This figure shows that the worst case scenario, with a lower cross-over frequency and stability margin, appears in nominal operation.

4.2. Maximum current loop

In this case, the control loop relates the maximum amplitude phase current to the rated current I_{rated}. Additionally, controlling I_q^+ ensures that the maximum amplitude current reaches the rated value required by objective 3. Fig. 8 shows the block diagram for the small-signal analysis. The amplitudes of natural frame currents can be written as a function of the current sequence components I_p, I_q^+, and I_q^-, and the phase angle between positive and negative current sequences $\phi_i = \{\delta_i, \delta_i - 2/3\pi, \delta_i + 2/3\pi\}$ as

$$I_{a,b,c} = \sqrt{\left(I_p\right)^2 + \left(I_q^+\right)^2 + \left(I_q^-\right)^2 + 2\sqrt{\left(I_p\right)^2 + \left(I_q^+\right)^2} I_q^- \cos\left(\phi_i\right)} \cdot \quad (21)$$

Following the approach used in the previous subsection, (21) can be linearized around small variations over the operating point:

$$\hat{I}_{Max}(s) = \frac{I_{q\,op}^+ + \frac{I_{q\,op}^- I_{q\,op}^+ cos_{\,iM\,op}}{\sqrt{A}}}{\sqrt{A + \left(I_{q\,op}^-\right)^2 + 2\sqrt{A} I_{q\,op}^- cos_{\,iM\,op}}} \hat{i}_q^+(s) \quad (22)$$

$$A = \left(I_{p\,op}\right)^2 + \left(I_{q\,op}^+\right)^2 \quad (23)$$

where $cos_{iM\,op}$ is the maximum cosine value (i.e. the cosine that produces the maximum amplitude in (21)). When choosing the PI gains as $k_{p\_i} = 0.6$ and $k_{i\_i} = 130\ s^{-1}$, a phase margin PM = 45º is obtained for the worst case scenario [$I_{p\,op}$, $I^+_{q\,op}$, $I^-_{q\,op}$] = [0, 1, 0] p.u. Fig. 9 shows the Bode plot of the loop gain for different sets of current components.

5. Experimental results

To evaluate the proposed control scheme using experimental results, a prototype rated at 1.4 kVA was built using a SEMIKRON full-bridge. A dc-source emulates the DGS. The grid is emulated with a programmable three-phase ac-source connected to the PCC with coupling inductors emulating the grid impedance. The LCL filter component values have been designed using the procedure described in [36]. A TMS320F28335 floating-point digital signal processor (DSP) was chosen as the control platform. The positive and negative-sequence extractor is based on a cascaded SOGI [34]. A rms algorithm implemented using a sliding-window calculates the phase currents and voltages values. The window-width of this moving average filter is a grid period, which generates a rms measure with a delay of 16.6 ms. Once the reference currents are calculated by using the proposed control scheme the driving signals for the power switches are generated by a proportional-resonant (PRES) current controller and a space vector PWM.

Table 2 lists the parameter values of the inverter and controller. A high value of the line inductance (0.073 p.u.) is chosen to clearly show the capability for voltage restoration of the inverter.

5.1. Low Active Power Production Scenario

A type II voltage sag was programmed in the ac-source to evaluate the behaviour of the system under a static sag. Fig. 10 shows the PCC phase-to-neutral voltages (top) and its rms per unit values (bottom) when the control is inactive.At the beginning of the test, during 0.15 seconds, the grid voltages are slightly unbalanced with the following rms voltages: 1.035 p.u., 0.994 p.u. and 1.035 p.u. At time t = 0.15 s the sag appears and the PCC voltages show constant amplitude until the fault is cleared, at t = 0.35 s, and the voltages recover their pre-fault values. Two dashed lines at 1.1 p.u. and 0.85 p.u. are drawn horizontally to highlight the voltage boundaries. As it can be seen, the voltage in phase c (in magenta) has fallen below the continuous operation limits, triggering the sag controller. On the other hand, phase a (in green) is slightly below the maximum voltage limit (1.1 p.u.).

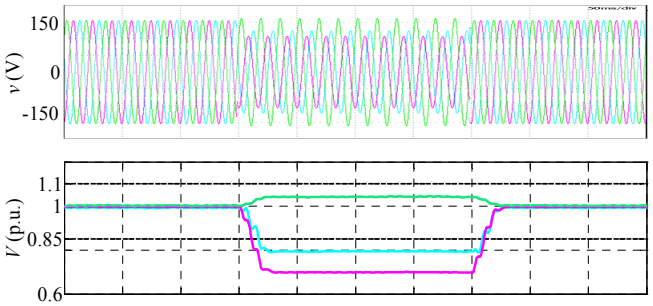

Fig. 10. Measured PCC phase voltages when the control is inactive. Top: phase voltages, bottom: rms per unit amplitudes. Phase a in green, b in blue, c in magenta (50 ms/div).

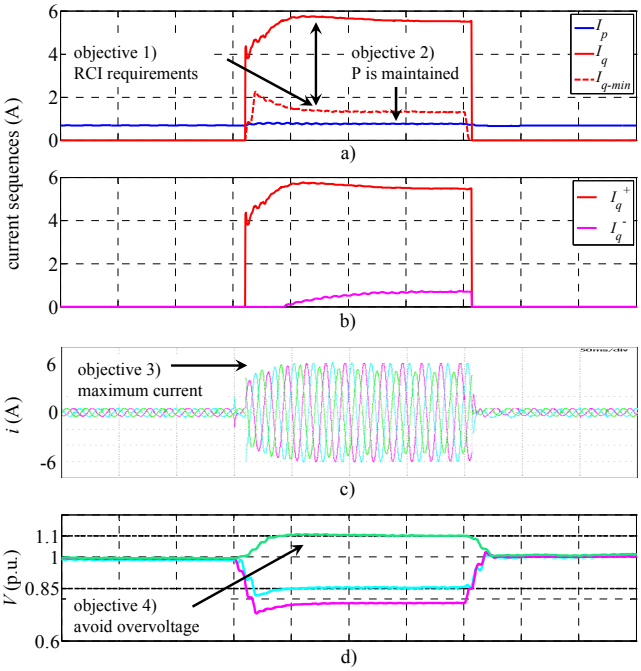

Fig. 11. Measurements in the low production scenario PG = 100 W. a) Active and reactive currents. b) Reactive sequence currents. c) Instantaneous phase currents, phase a in green, b in blue, c in magenta. d) Phase voltages rms per unit amplitudes. (50 ms/div).

Depending on the amount of reactive current injection, this upper limit could be exceeded, thus worsening the voltage profile. In this test, two active power generation values have been considered, 100W and 1100W, in order to show two different scenarios: the first one with enhanced support capabilities due to the high reactive current injection, and the second one, where only positive-sequence reactive current is injected.

First, the low active power generation is considered, P_G = 100 W. Fig. 11 a) and b) shows the instantaneous current measurements and its active/reactive positive/negative-sequence components. Before the sag, the inverter is injecting a low active current with a peak value of 0.3 A.

When the sag is detected, the reactive power injection begins with a large positive-sequence current amplitude, as shown in Fig. 11 a) and b). This amplitude produces the same increment in the voltages of the three phases. In the top sub-figure, the minimum reactive current required by the grid code I_{q_min} is shown as a dashed line. If this value had been

used for the current injection, the objective of maximizing the power capability of the inverter would have not been accomplished. Thanks to the proposed control algorithm, the positive-sequence reactive current grows until the maximum phase current I_{rated} is reached (clearly I_q is higher than $I_{q\ \min}$). Before t = 0.19 s the currents are balanced due to the unique reactive current injection via positive-sequence. As an undesired effect, the high balanced reactive current injection brings phase *a* voltage (in green, the non-dropped phase) above the upper limit set to 1.1 p.u. Thus, when this limit is reached (at approximately t = 0.19 s), the inverter starts injecting reactive current also through negative-sequence (see middle sub-figure) trying to equalize the phase voltages, i.e. reducing the higher voltage with the aim of not crossing the upper limit. At the same time positive-sequence of the reactive current is reduced slightly by the controller to avoid exceeding the maximum rated-current of the inverter. Fig. 11 c) shows the instantaneous measured currents, kept to the maximum rated current of 6A as required. It must be noted that when I_q^- appears and due to its unbalancing effect, phase *a* current (in green) presents the minimum amplitude value, as expected (i.e. produces the minimum increment in the grid inductance). Also, it must be highlighted that phase *c* current (in magenta) presents the maximum value (6 A), thus supporting to the maximum extent the most dropped voltage (i.e. phase *c*).

Fig. 11 d) shows the PCC voltages when the proposed control is activated. As it can be seen, phase *a* voltage (in green) quickly reaches the upper limit 1.1 p.u. after the control starts the reactive-current injection. Thanks to the particular injection of negative-sequence reactive current, this limit is not exceed. It can be noted that the sag cannot be supported completely (i.e. to raise the lower phase voltages to the continuous operation boundaries) due to the low power rating of the inverter. However, it is clear that using the proposed control scheme, the lower boundary for continuous operation will be reached with a high power rating inverter or when an array of low power rating inverters operating dispersedly share the same PCC. Note that the proposed control can also be used for the inverters described in these scenarios.

Finally, the fulfillment of the four proposed objectives can be clearly seen in the text boxes and arrows added to Fig. 11.

5.2. High Active Power Production Scenario, Active Power Curtailment

In the second experiment, a high active power generation is considered, P_G = 1100 W, under the same static sag shown in Fig. 10. Before the sag, active currents are balanced around a 5 A peak value, near to the inverter maximum current I_{rated} = 6 A. Fig. 12 a) and b) show the measured instantaneous current and its active/reactive positive/negative-sequence amplitudes. When the sag is detected, the controller begins the reactive current injection via positive-sequence, reaching a peak value of 2.2 A when the maximum rated current starts being injected. In this case, the minimum reactive current to be injected (dashed line) is clearly exceeded during the first part of the sag. Hence, the best use of the inverter power capability is achieved, accomplishing the three current objectives simultaneously.

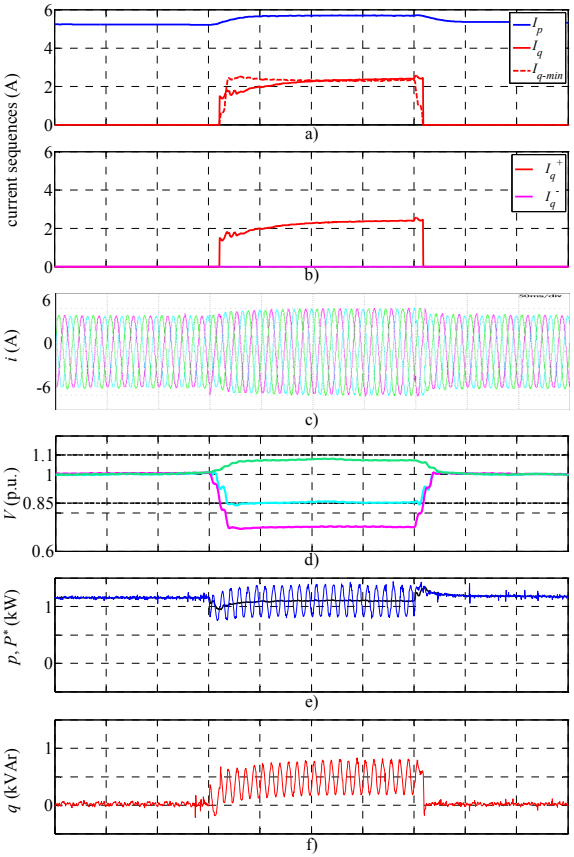

Fig. 12. Measurements in the high production scenario P_G = 1100 W. a) Active and reactive currents. b) Reactive sequence currents. c) Instantaneous phase currents, phase a in green, b in blue, c in magenta. d) Phase voltages rms per unit amplitudes. e) Instantaneous active power in blue, reference active power in black. f) Reactive power. (50 ms/div).

As it can be seen in the figure, the current amplitudes are always balanced because no injection is performed via negative-sequence (I_q^- = 0), and therefore kept to the maximum rated current, 6A. The negative-sequence current is zero because the maximum voltage does not reach the upper limit, 1.1 p.u. (see Fig. 12 d)) and then, the maximum voltage PI compensator is saturated at its lower limit. Due to the fact that the reference power P^* is kept stable during the sag, the active current Ip grows in order to compensate the drop in phase c voltage. As it will be explained later, some active power curtailment is necessary to observe the ratio I_q/I_T required by the grid code.

Fig. 12 d) shows PCC voltages when the proposed control is active. As it can be seen, phase *a* voltage does not reach the upper limit 1.1 p.u., and no negative-sequence current injection is required. Fig. 12 e) shows the injected active power (in blue) and the reference active power P^* (in black). The power curtailment action necessary to fulfill the grid code can also be seen (note the 50 W reduction in P^*). Fig. 12 f) shows the low value of the instantaneous reactive power injected, with a mean value of 500 VAr.

5.3. Supporting variable-profile sags

A variable-profile voltage sag, shown in Fig. 13, was also programmed in the ac-source to evaluate the behavior of the proposed control scheme. In particular, the sag with slow

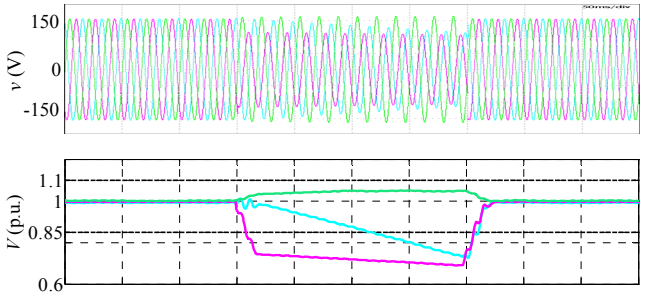

Fig. 13. Dynamic sag. Measured PCC phase voltages when the control is inactive. Top: phase voltages, bottom: rms per unit amplitudes. Phase a in green, b in blue, c in magenta (50 ms/div).

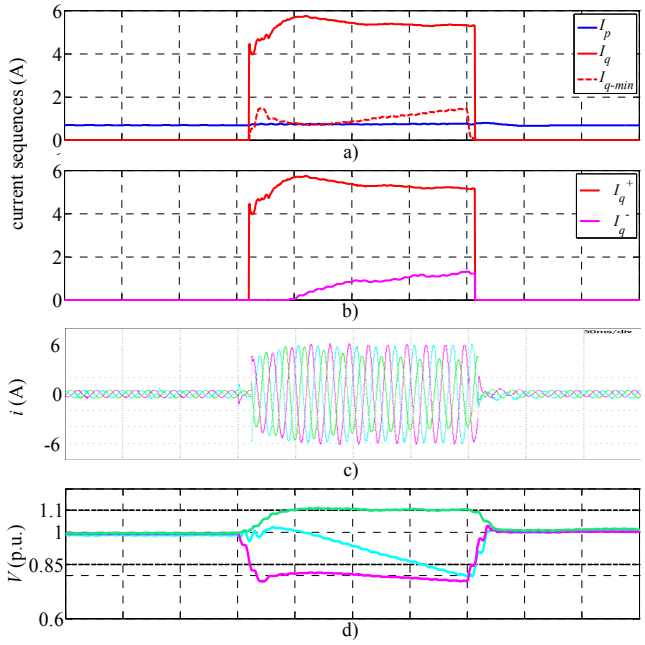

Fig. 14. Dynamic sag. Measurements in the low production scenario PG = 100 W. a) Active and reactive currents. b) Reactive sequence currents. c) Instantaneous phase currents. d) Phase voltages rms per unit amplitudes. (50 ms/div).

dynamics described in [10] is reproduced here due to its complex profile. Initially, its behavior corresponds to a type I sag with one dropped voltage [23]. After a short time, phase *b* voltage (in blue) begins to drop evolving to a type II sag before it is cleared. In this third experiment, only a low active power generation scenario is considered, P_G = 100 W. Fig. 14 a) and b) show the active/reactive positive/negative-sequence components. Fig. 14 c) shows the instantaneous current measurements. When the sag is detected, the reactive power injection starts with a high positive-sequence current amplitude, as shown in Fig. 14 a) and b). When phase *a* voltage (in green) reaches 1.1 p.u due to the injection of positive-sequence reactive current, negative current injection starts taking place. I_q^+ decreases and I_q^- increases following the variable profile of the sag. As it can be seen at Fig. 14 c) the currents are safely kept to a 6A peak value. In this sub-figure, the accomplishment of objective 3, i.e. inject maximum reactive current in the phase with lowest voltage, can be clearly observed: phase *c* (magenta) current always presents the maximum amplitude. Fig. 14 d) shows PCC

Table 3 Comparison with previous strategies

Ref.	Over current control	Maxim. RCI	Voltage support	Voltage control	P Q inject.	Active power curt.	CB
[21], 2013	×	×	✓	×	Q	×	↓
[23], 2013	×	×	✓	✓	Q	P = 0	↑
[22], 2014	×	×	✓	×	P & Q	×	↓
[24], 2014	✓	×	✓	✓	Q	P = 0	↑
[25], 2014	✓	×	✓	✓	Q	P = 0	↔
[13], 2015	✓	×	×	×	P & Q	✓	↔
[18], 2015	✓	×	×	✓	Q	P = 0	↑
[29], 2015	✓	✓	✓	✓	Q	P = 0	↑
[30], 2015	✓	×	✓	×	P & Q	✓	↓
[14], 2016	✓	✓	×	×	P & Q	✓	↔
[15], 2018	✓	✓	×	×	P & Q	✓	↔
Proposal	✓	✓	✓	✓	**P & Q**	✓	↓

voltages when the proposed control is activated. As it can be seen, the maximum voltage is kept safely in the high boundary of continuous operation mode. From the previous results, it can be concluded that the proposed control is able to meet the control objectives in representative production scenarios, including low and high power production and it offers a better use of the reactive power provision of full-power inverters.

From the previous results, it can be concluded that the proposed control is able to meet the control objectives in representative production scenarios, including low and high power production and it offers a better use of the reactive power provision of full-power inverters.

6. Comparison to previous control schemes

Table 3 presents a comprehensive comparison between previous state-of-the-art controllers and the proposed one. As stated above, the presented scheme combines some interesting objectives: it applies maximum RCI to the phase affected by the highest fault, it activates active power curtailment only whenever required, and it avoids exceeding the upper-voltage limit. In contrast, some of state-of-the-art schemes reach similar objectives but independently, without combining them in a single controller. Also, the computational burden (CB) is very low compared to other approaches thanks to the use of simple PI controllers. For example, the control scheme proposed in [29] that offers similar features to the one proposed in this paper is more costly than the one here presented. The proposed one requires only 6 square roots and 32 sums/products to complete the control algorithm (approximately 6 µs). The algorithm in [29] computes 7 square roots, 49 sums/products, 2 angle calculations and 5 divisions, resulting in a computational effort of roughly 18 us. It is worth mentioning that the algorithm required to calculate the grid impedance in [29] is not considered in this estimation. Thus, the improvement of the proposed control scheme is even more significant. The other work that presents a multi objective controller is [30], although the interesting purpose of injecting the maximum allowable reactive current is not presented and no closed-loop voltage control is proposed.

7. Conclusions

This paper proposes an adjustable positive/negative-sequence reactive current injection scheme for grid-

connected inverters under voltage sags. Thanks to the flexible sequences injection, at least one phase current is maintained at its maximum rated value, thus providing maximum support to the most faulted phase voltage. Active power curtailment is applied only when it is required by the grid code. As an additional feature, a voltage control loop was implemented to avoid overvoltage in non-faulty phases due to the reactive current injection. Further analysis on the performance of the proposed control scheme is open for future research. Specially, to avoid the inherent drawbacks of PI controllers working in a highly non-linear power network. Additional research in advanced non-linear controllers could enhance the features of the proposal.

8. References

[1] Blaabjerg, F., Teodorescu, R., Liserre, M. et al.: 'Overview of control and grid synchronization for distributed power generation systems'. IEEE Trans. Ind. Electron., 2006, 53, (5), pp. 1398–1409

[2] IEC Std. 61727–2004: 'Characteristics of the utility interface for photovoltaic systems', 2004

[3] IEEE Std. 1547.2-2008: 'IEEE Application Guide for IEEE Std 1547, IEEE Standard for Interconnecting Distributed Resources with Electric Power Systems', 2009

[4] Red Electrica, 'Resolution-P.O.12.3-Response requirements against voltage dips in wind installations' (Red Electrica Española, 2006)

[5] Gobierno de España, 'P.O.12.2 Technical requirements for wind power and photovoltaic installations and any generating facilities whose technology does not consist on a synchronous generator directly connected to the grid' Offprint from the O.P. 12.2 outline. Oct. 2008.

[6] Altin, M., Goksu, O., Teodorescu, R. et al.: 'Overview of recent grid codes for wind power integration'. in 12th Int. Conf. on Optimization of Electrical and Electronic Equipment, Brasov, Romania, May 2010, pp. 1152–1160

[7] Tsili, M., Papathanassiou, S.: 'A review of grid code technical requirements for wind farms'. IET Renew. Power Gen., 2009, 3, (3), pp. 308–332

[8] Troester, E.: 'New German grid codes for connecting PV systems to the medium voltage power grid'. in Proc. 2nd Int. Workshop Concentrating Photovoltaic Power Plants, Mar. 2009, pp. 1–4

[9] Bollen, M.H.: 'Understanding power quality problems: Voltage sags and interruptions' (IEEE Press, 2000)

[10] Cundeva, S., Neumann, R., Bollen, M.H., et al.: 'Immunity against voltage dips – Main recommendations to stakeholders of the CIGRE/CIRED/UIE Joint Working Group C4.110'. Int. J. Emerg. Sci., 2011, 1, (4), pp. 555–563

[11] Miret, J., Castilla, M., Camacho, A. et al.: 'Control scheme for photovoltaic three-phase inverters to minimize peak currents during unbalanced grid-voltage sags'. IEEE Trans. Power Electron., 2012, 27, (10), pp. 4262–4271

[12] Lee, C.-T., Hsu, C.-W. and Cheng, P.-T.: 'A low-voltage ride-through technique for grid-connected converters of distributed energy resources'. IEEE Trans. Ind. Appl., 2011, 47, (4), pp. 1821–1832

[13] Camacho, A., Castilla, M., Miret, J. et al.: 'Active and reactive power strategies with peak current limitation for distributed generation inverters during unbalanced grid faults'. IEEE Trans. Ind. Electron., 2015, 62, (3), pp. 1515–1525

[14] Sosa, J.L., Castilla, M., Miret, J. et al.: 'Control strategy to maximize the power capability of PV three-phase inverters during voltage sags'. IEEE Trans. Power Electron., 2016, 31, (4), pp. 3314–3323

[15] Garnica Lopez, M.A., Garcia de Vicuna, J.L., Miret, J. et al.: 'Control Strategy for grid-connected three-phase inverters during voltage sags to meet grid codes and to maximize power delivery capability'. IEEE Trans. Power Electron., 2018, early access article

[16] Chen, H.-C., Lee, C.-T., Cheng, P.-T. et al.: 'A low-voltage ride-through technique for grid-connected converters with reduced power transistors stress'. IEEE Trans. Power Electron., 2016, 31, (12), pp. 8562–8571

[17] Nejabatkhah, F., Li, Y., and Wu B.: 'Control strategies of three-Phase distributed generation inverters for grid unbalanced'. IEEE Trans. Power Electron., 2016, 31, (7), pp. 5228–5241

[18] Milicua, A., Abad, G., and Rodriguez-Vidal, M.A.: 'Online reference limitation method of shunt-connected converters to the grid to avoid exceeding voltage and current limits under unbalanced operation—Part I: Theory'. IEEE Trans. Energy Convers., 2015, 30, (3), pp. 852–863

[19] Milicua, A., Abad, G., and Rodriguez-Vidal, M.A.: 'Online reference limitation method of shunt-connected converters to the grid to avoid exceeding voltage and current limits under unbalanced operation—Part II: Validation'. IEEE Trans. Energy Convers., 2015, 30, (3), pp. 864–873

[20] Shabestary, M.M., and Mohamed, Y.: 'Analytical expressions for multi-objective optimization of converter-based DG operation during unbalanced grid conditions'. Trans. Power Electron., 2017, 32, (9), pp. 7284–7296

[21] Camacho, A., Castilla, M., Miret, J. et al.: 'Flexible voltage support control for three-phase distributed generation inverters under grid fault'. IEEE Trans. Ind. Electron., 2013, 60, (4), pp. 1429–1441

[22] Guo, X., Zhang, X., Wang, B. et al.: 'Asymmetrical grid fault ride-through strategy of three-phase grid-connected inverter considering network impedance impact in low-voltage grid'. IEEE Trans. Power Electron., 2014, 29, (3), pp. 1064–1068

[23] Miret, J., Camacho, A., Castilla, M. et al.: 'Control scheme with voltage support capability for distributed generation inverters under voltage sags'. IEEE Trans. Power Electron., 2013, 28, (11), pp. 5252–5262

[24] Camacho, A., Castilla, M., Miret, J. et al.: 'Reactive power control for distributed generation power plants to comply with voltage limits during grid faults'. IEEE Trans. Power Electron., 2014, 29, (11), 2624–2634

[25] Castilla, M., Miret, J., Camacho, A. et al.: 'Voltage support control strategies for static synchronous compensators under unbalanced voltage sags'. IEEE Trans. Power Electron., 2014, 29, (11), pp. 6139–6150

[26] Goksu, O., Teodorescu, R., Bak, C.L. et al.: 'Impact of wind power plant reactive current injection during asymmetrical grid faults'. IET Renew. Power Gen., 2013, 7, (5), pp. 484–492

[27] Dai, Z., Lin, H., Yin, H. et al.: 'A novel method for voltage support control under unbalanced grid faults and grid harmonic voltage disturbances'. IET Power Electron., 2015, 8, (8), pp. 1377–1385

[28] Neumann, T., Wijnhoven, T., Deconinck, G. et al.: 'Enhanced dynamic voltage control of type 4 wind turbines

during unbalanced grid faults'. IEEE Trans. on Energy Conv., 2015, 30, (4), pp. 1650–1659

[29] Miret, J., Camacho, A., Castilla, M. et al.: 'Reactive current injection protocol for low-power rating distributed generation sources under voltage sags'. 2015, IET Power Electron., 8, (6), pp. 879–886

[30] Mirhosseini, M., Pou, J., and Agelidis, V.G.: 'Individual phase current control with the capability to avoid overvoltage in grid-connected photovoltaic power plants under unbalanced voltage sags'. IEEE Trans. Power Electron., 2015, 30, (10), pp. 5346–5351

[31] Teodorescu, R., Liserre, M., and Rodríguez, P.: 'Grid converters for photovoltaic and wind power systems' (John Wiley & Sons 2011)

[32] Figueres, E., Garcera, G., Sandia, J. et al.: 'Sensitivity study of the dynamics of three-phase photovoltaic inverters with an LCL grid filter'. IEEE Trans. Ind. Electron., 2009, 56, (3), pp. 706–717

[33] Liserre, M., Teodorescu, R. and Blaabjerg, F.: 'Stability of photovoltaic and wind turbine grid-connected inverters for a large set of grid impedance values'. IEEE Trans. Power Electron., 2006, 21, (1), pp. 263-272

[34] Matas, J., Castilla, M., Miret, J. et al.: 'An adaptive pre-filtering method to improve the speed/accuracy trade-off of voltage sequence detection methods under adverse grid conditions'. IEEE Trans. Ind. Electron., 2014, 61, (5), pp. 2139–2151

[35] Mirhosseini, M., Pou, J., and Agelidis, V.G.: 'Single- and two-stage inverter-based grid-connected photovoltaic power plants with ride-through capability under grid faults'. IEEE Trans. Sust. Energy, 2015, 6, (3), pp. 1150–1159

[36] Liserre, M., Blaabjerg, F., and Hansen, S.: 'Design and control of an LCL filter-based three-phase active rectifier'. IEEE Trans. Ind. Appl., 2005, 41, (5), pp. 1281–1291